SIMPLIFIED 3D CFD FLOW SIMULATION OF A TURBOJET DISC CAVITY WITH CONJUGATE HEAT TRANSFER

ISABE-2003-

Glen C. Snedden
CSIR, Defencetek, P O Box 395
Pretoria, 0001, South Africa
Tel: +2712 841-3094
Fax: +2712 349-1156
gsnedden@csir.co.za

Abstract

A comprehensive computational fluid dynamics (CFD) model of an actual disc cavity, complete with rotation and conjugate heat transfer, is presented. The model uses a commercially available code with geometrical accuracy including a labyrinth seal, all the physics of a rotating system and conjugate heat transfer. Results presented include: flow patterns, pressure distributions and temperature distributions in both the fluid and metal components, as well as heat transfer. Validation results for the temperature of the 1st rotor disc are also presented.

Introduction

The need for accurate solutions of the disc metal temperature distributions in gas turbines stems largely from the desire for more accurate boundary conditions for the life assessment of highly stressed turbine components.

In the past, hardware limitations at Defencetek restricted the Navier-Stokes modelling of disc cavities and other complex geometries to relatively few cells. Assumptions about areas such as the labyrinth seal and even the geometry of the disc cavities were forced on users. The extents of these assumptions meant that very often what results were obtained were unphysical. A more accurate approach wherein a detailed geometrical model was generated using all the drawings available to Defencetek and a combination of Computer Aided Design (CAD) and the commercial Navier-Stokes solver - Star-CD, operating on workstations, was followed. This combination led to the model presented in this paper.

This work represents a method to obtain detailed flow patterns, temperature and pressure distributions in highly complex rotational systems using commercial software and at relatively low cost.

However, it is also clear that increased computational capacity is necessary to attempt higher accuracy modelling of heat transfer using the recommended near wall Reynolds numbers, that is, sufficient mesh refinement in the boundary layer region.

Model Geometry

Modelling Approach

A two-dimensional radial section (Figure 1) of the disc geometry was pieced together in CAD from part drawings, and divided into blocks. The definition of blocks is dictated largely by user experience and the requirement to have exact cell matching wherever possible. This process led to a total of over three hundred discrete mesh blocks.

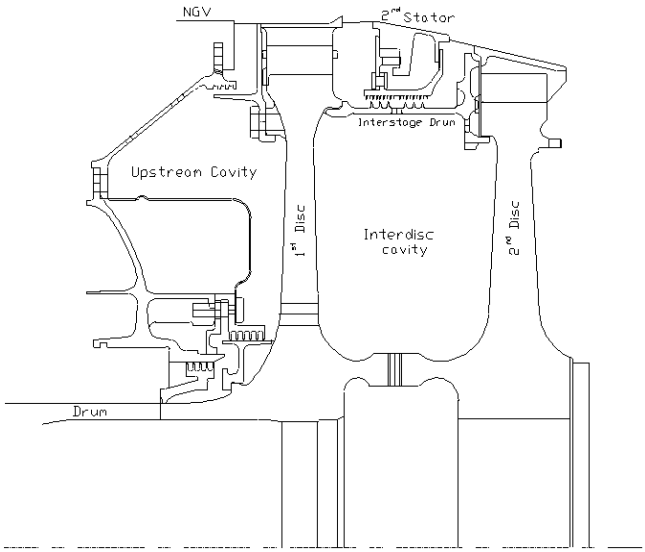

Figure 1: CAD assembly of part drawings

A data file containing all the necessary coordinates and other block details was then extracted from CAD and converted to Star-CD commands using a Fortran routine. This provided a semi-automated modelling process, which means that changes to the final Star-CD model are quickly implemented.

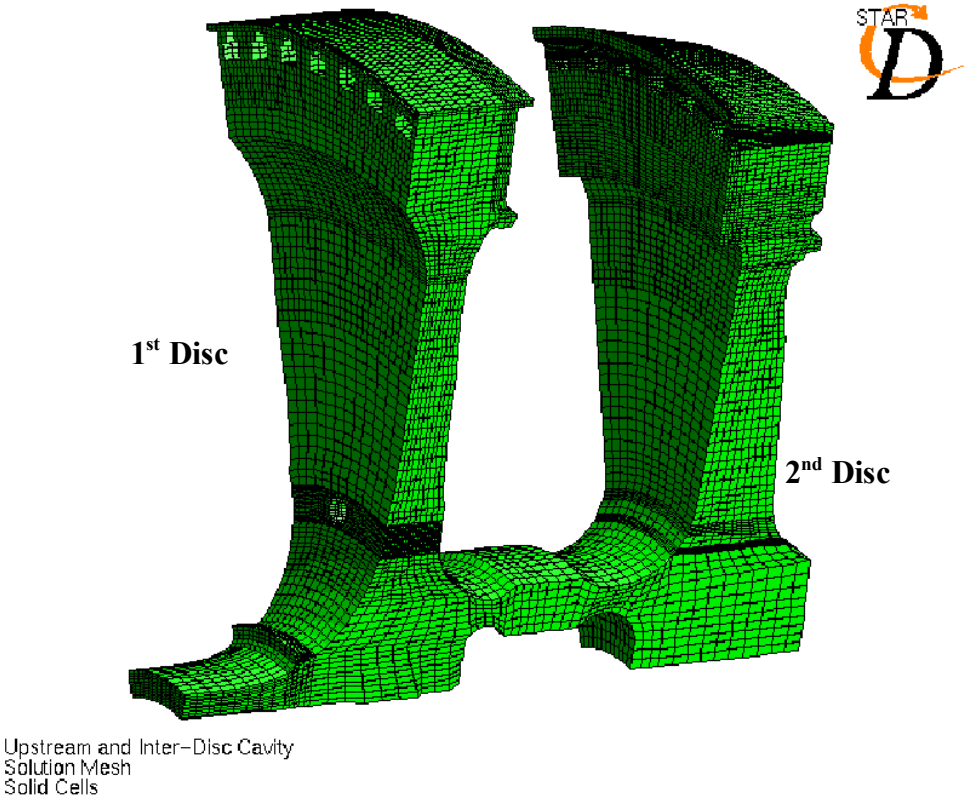

Figure 2: Disk geometry

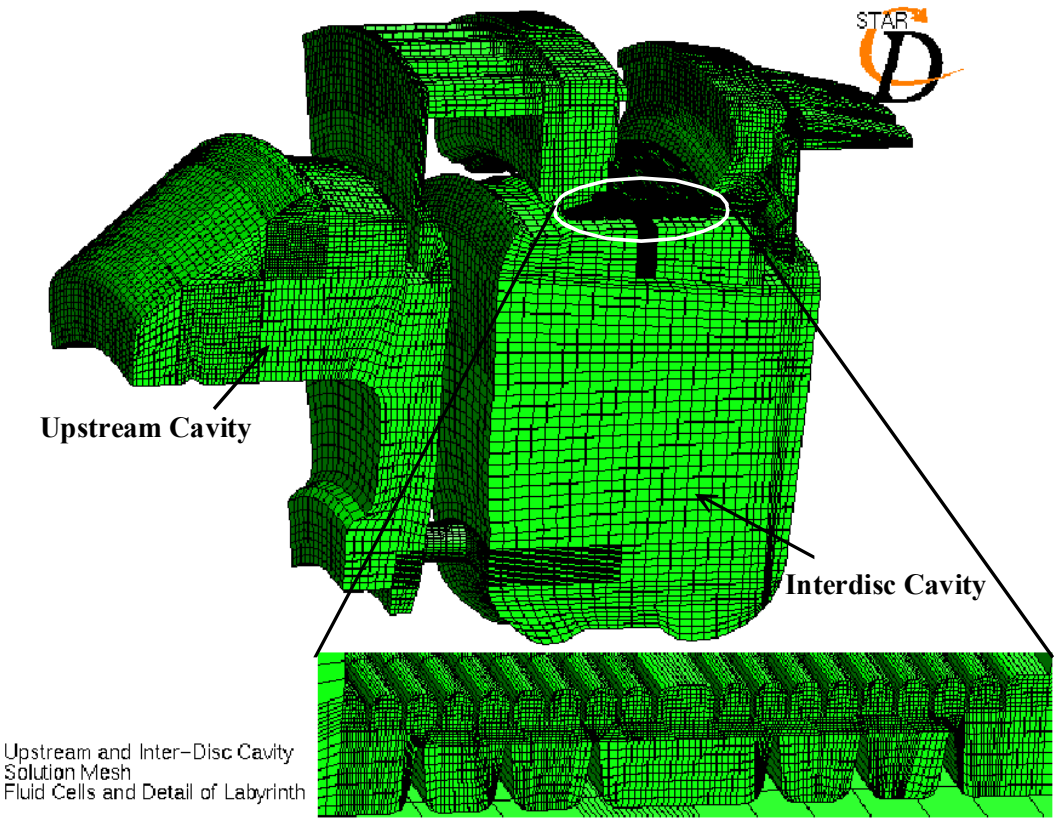

Figure 3: Fluid cell geometry

To reduce the overall mesh size, a 30° wedge of the disk cavity was modelled instead of the full cavity. A finite size wedge angle was chosen as the fluid flow is not purely two-dimensional in the radial plane but periodic behaviour is created by a non-axisymmetric geometry. The geometry includes 12 large axial cooling holes at mid-radius of the first rotor disk, 83 first stage rotor blades with corresponding gaps between the root shanks and 66 second stage rotor blades, with similar inter-shank holes.

The 30° wedge was chosen in order to capture one of the 12 large axial holes in the first rotor disk. For the purposes of the simulation, the 83 rotor blades were artificially increased in number to 84 to allow an integer number (7) of blade shank gaps, and the 66 blades of the second stage were increased to 72 to give 6 gaps by the same token. This modelling configuration allowed the use of cyclic boundary conditions.

Final mesh statistics are as follows:

- More than 220 000 fluid cells
- In excess of 58 000 solid cells

Geometrical Assumptions

Assumptions were necessary with regard to the physical positioning of some components. All radial positions are correct as they are provided in the part drawings. Axial positioning, however, is a matter of more concern, as no assembly drawings were available to the author. Where no physical contact between parts is available to indicate axial positioning, the author had to rely on experience and sketches from the engine user manual. These areas include the upstream assembly, inter-disc drum and second stage stator base. Leakage flow from the main gas flowpath into the intershank cavities in the 2nd disc was eventually closed with a baffle as no gap was evident in the physical engine.

For simplicity, passages under the rotor blade platforms between the blade root shanks and above the actual disc are modelled by changing existing solid cells to fluid cells in such a way that no changes in the actual geometry of the mesh are introduced. At the same time hole numbers, shape and size are not entirely accurate, as explained in Modelling approach (these 'holes' are clearly visible in Figures 2 and 3). Where hole numbers were changed their individual sizes were modified so that the sum of their areas across the 12 sectors would approximate that of the actual geometry. Furthermore, the blade material and disc material in the fir tree region are assumed to be homogeneous and uninterrupted, that is, thermal contact resistance was not modelled.

The 30° wedge, as mentioned previously, was based on the number of holes through the first stage disc; this does not allow for the various other holes. These include fifteen holes into the labyrinth seal area and twenty holes through the rear of the inter-disc drum. To solve this problem, the areas of these holes were adjusted to conserve mass-flow and only one hole into the labyrinth and two through the drum were modelled in the 30° wedge.

A final assumption was that all bolt heads and a raised lug on the upstream side of the first rotor disc were removed from the final model.

Figures 2 and 3 show the final mesh used in the solution, solid and fluid cells respectively.

Boundary Conditions and Assumptions

Two assumptions about flow in the upstream cavity greatly simplify the final model. Firstly, no flow enters or leaves via the labyrinth seals close to the hub, upstream of the first disc (refer to Figure 1). This assumption is well founded as the seal has close tolerances and consists of two serial sections of seal. The second assumption is that there is no flow through the top of the seal under the nozzle guide vane (NGV). As can be seen in Figure 1, the gap in this seal is large, however, it was felt that the small pressure difference between coolant air and NGV exit air would most likely be adequately blocked by coolant flow introduced through a series of small holes above the seal. The effects of thermal expansion have also not been accounted for and this should close the tolerances of all the labyrinth seals.

Two inlet boundaries (Figure 4), in reality two rows of holes connecting the cool pressurised outer combustor cavity with the upstream disk cavity, were modelled as thin slots introducing a constant mass-flow (approximately 0.35% of engine mass-flow each).

This mass-flow is obtained from a realistic approximation of the flow split between NGV cooling and disc coolant, with the total coolant percentage given as 2.7% of overall mass-flow by the engine user manual. Modelling the inlets as a single row of cells is justified by their position, that is, far away from the actual areas of interest, as well as the significant simplification of the model, as sliding meshes are avoided. Furthermore, the discrete inlet holes are modelled as slots. It was felt that this actually simulated the effect of the rotor moving past a series of stationary, discrete holes. Coolant inlet temperature was 531 K.

The temperatures of the rotor blade platforms (Figure 4) are modelled as constant temperature areas using temperatures obtained from flow field values close to the hub of the respective blade rows, thus ignoring the thermal resistances created by the heat transfer coefficients. The temperatures are 1061 K and 964 K respectively, and were obtained from a previous re-engineering exercise using the TD3D code (NREC, 1972) to obtain flow temperatures and pressures through the main gas flow path of the turbine.

Using temperatures and pressures obtained in a similar fashion, pressure boundaries were specified between the discs and the second stage stator as well as at the exits to the holes in the second disc (Figure 4).

Turbulence was modelled using the standard k-ε model available to Star-CD users. Boundary values at inlet and pressure boundaries were all specified as 5% intensity and having length scales approximately one tenth of the hole diameter. As is clear from the coarse nature of the grid, no attempt was made to reduce near wall Reynolds numbers to the recommended levels of less than 1 (CD Limited, 1999) in the boundary layer regions close to the wall. This is impossible in the light of mesh size limitations imposed by hardware constraints circa 1999.

All wall boundaries are default, as Star-CD automatically assigns spin parameters to walls in spinning 'zones' and stationary walls in zones without spin velocities. Furthermore, wherever fluid does not touch the solid, the wall is assumed adiabatic. This is considered to be acceptable in the absence of geometry and flow information through the hubs and over the back of the second disc. It must also be noted that, conduction across the inter-disc drum and across the second stage stator assembly were not modelled due to the lack of thermal contact resistance information.

This last assumption may well have strong consequences to the fluid solution through the labyrinth seal in particular.

The curvic-coupling between discs is assumed to be continuous, without thermal contact resistance, this too may be inaccurate, but simplified the mesh and is justified as no significant metal temperature gradient is expected across the coupling region.

Cyclic boundaries were placed on the radial sides of the wedge.

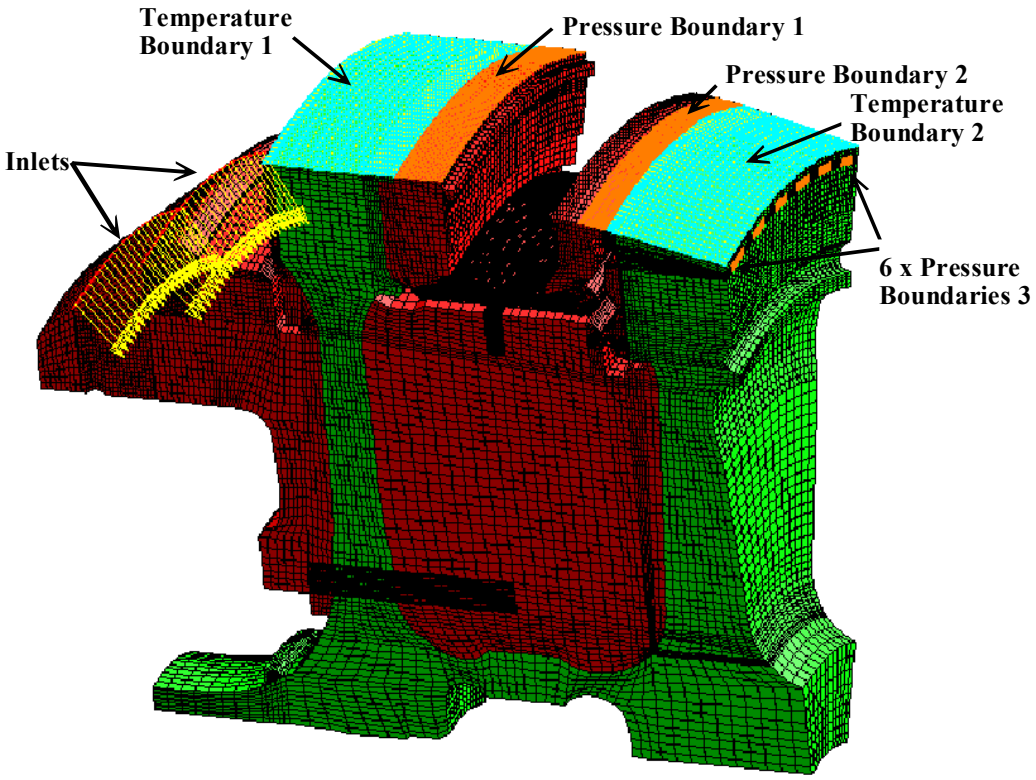

Figure 4: Overall geometry boundary conditions

Convergence And Materials Properties

Initial solutions with reduced mass flow at inlet, constant fluid density and low rotational velocities, provided a starting point for the final solution. A total of close to ten thousand iterations provided a clear convergence plot of all residuals. The final iterations to convergence used ideal gas law density calculations, Sutherland's law for viscosity and thermal conductivity (White, 1991) and a fifth order polynomial fit for specific heat capacity (Zucrow and Hoffman, 1976). These relationships ensure accuracy in the gas properties over a large range of temperatures.

Metal properties were assumed to be constant with temperature and those for Stainless Steel 316 were used. Actual disc material varied between discs, but both are some form of Discalloy, which exhibits similar thermal properties to those of 316 Stainless Steel.

Flow Solution

Figures 5 to 9 show a selection of overall and detailed flow patterns through the geometry. All plots are sections showing only the velocity components in the section plane.

Interesting features include the inlet jets and the large number of recirculation zones associated with them. In fact the upper jet is deflected by reflecting off its own recirculation flow (Figure 6).

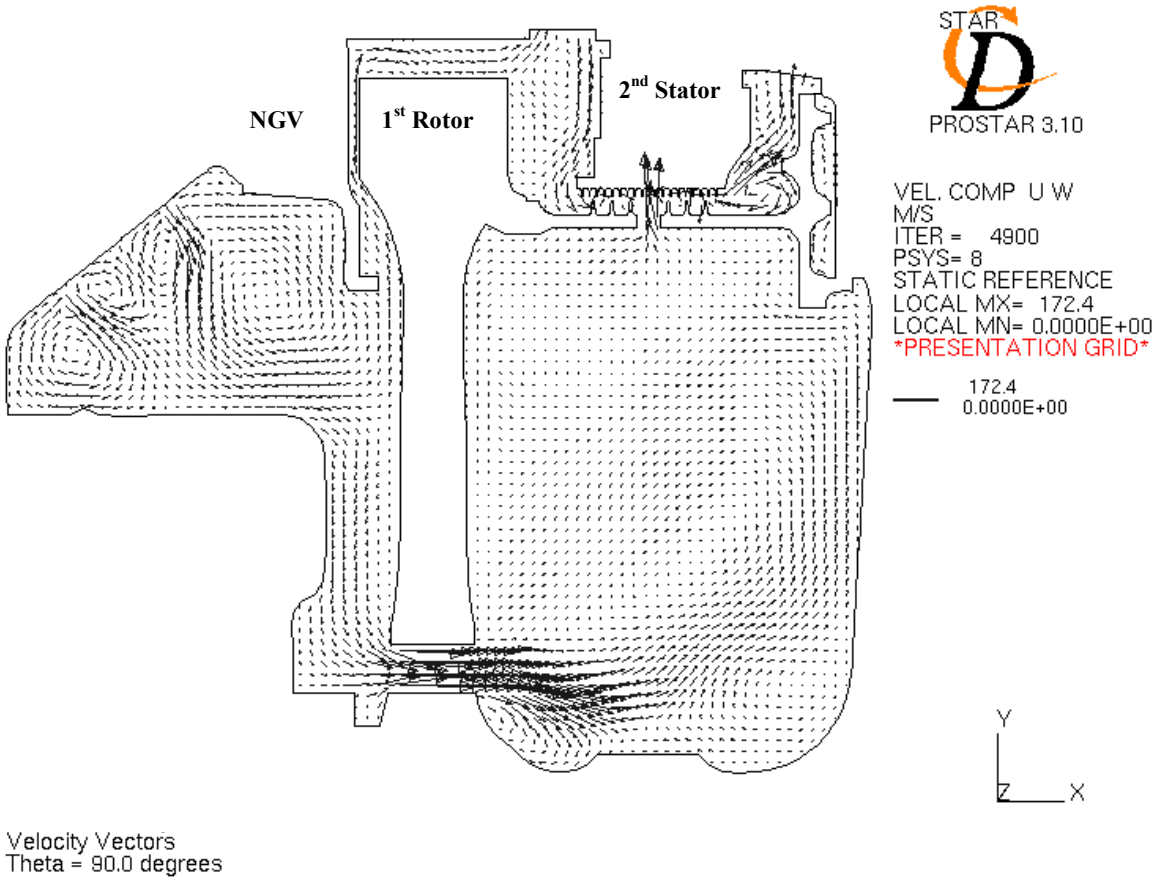

Figure 5: Overall flow pattern

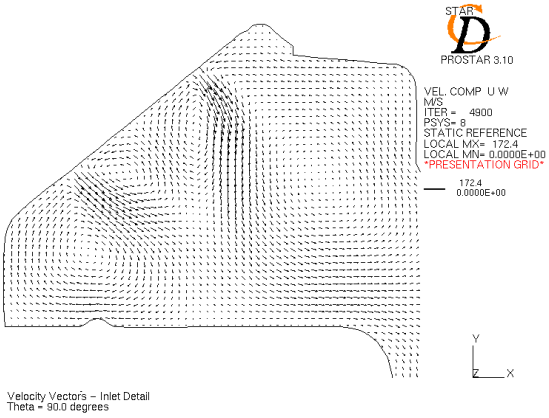

Figure 6: Inlet flow pattern

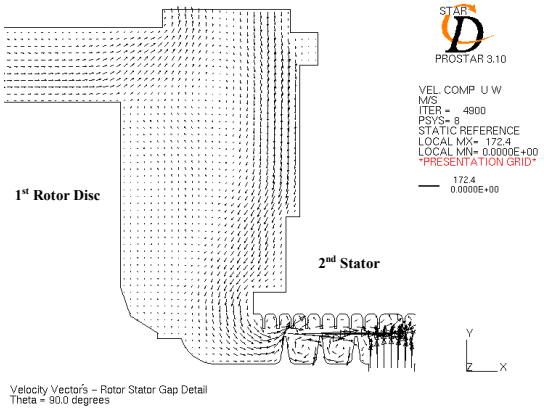

Figure 7: Overall flow pattern

There is clear evidence of centrifugal pickup of flow close to all three disc surfaces in the model. Figures 5 and 7 clearly show the fluid emerging from the holes under the blades of the first stage rotor being spun out through the pressure boundary, despite the fact that the remainder of the pressure boundary has flow entering the cavity.

Flow through the first disc clearly impinges on the second disc at approximately mid-radius, but is initially deflected leading to increased cooling close to the hub of the first disc. Figure 8 shows the strong impingement of flow onto the second disc just below the blade rotors. This accounts for the cold spots that will be seen in later results.

Flow through the second pressure boundary is predominantly out into the main gas flow path, driven by flow from upstream of the stator passing through the labyrinth seal and bringing coolant flow with it.

The labyrinth seal below the 2nd stator is shown in Figure 9, where flow patterns show clear recirculation zones in each groove of the seal, driven by the flow through the seal. The pressure plot included in this figure shows an overall pressure drop of some 54 KPa, although this is largely imposed by the specification of pressure boundaries.

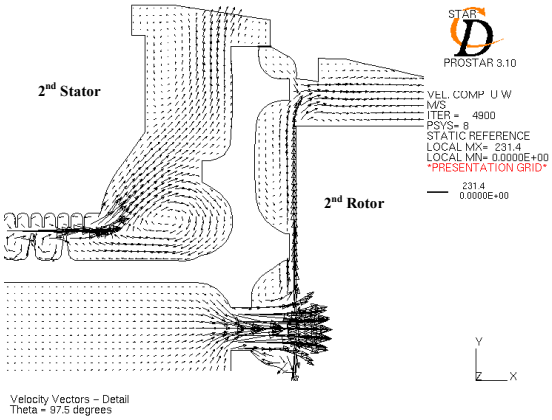

Figure 8: Flow pattern at second pressure boundary and through rear cooling holes

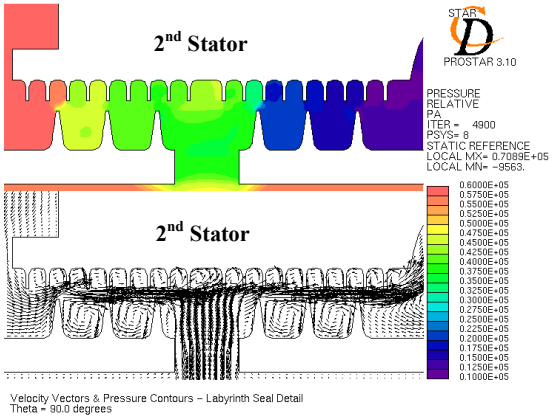

Figure 9: Labyrinth seal flow pattern and pressure drop

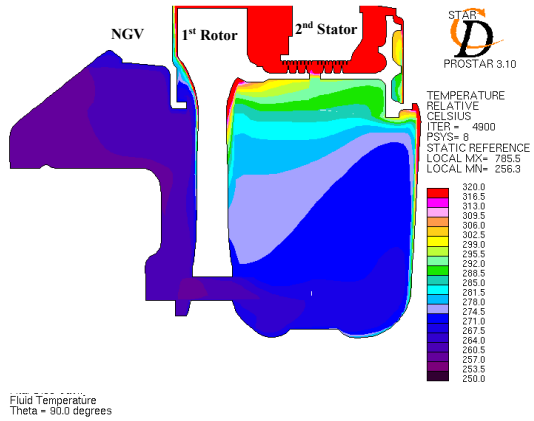

Figure 10: Fluid temperature

Temperature Solution

The plots of fluid temperature (Figure 10 and Figure 11) reveal little of any real interest. There is clear heat transfer to the fluid as one progresses closer to the top of discs. This is most evident in the inter-disc cavity on the downstream side of the disc. This region coincides with a near-stagnant region of flow (Figure 5). Coolant penetration into the inter-disc cavity is also clearly outlined. Accurate results in the boundary layer regions are precluded by the lack of sufficient grid refinement in these regions.

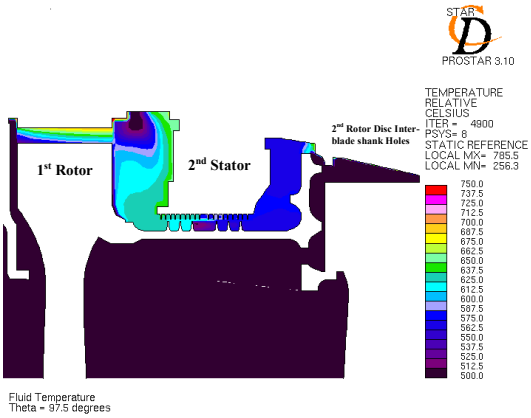

Figure 11: Fluid temperature, detail of Labyrinth seal

The detail plot of temperature in the labyrinth seal region (Figure 11) and through the coolant holes onto the second disc reveals that the ingress of hot gas through the holes beneath the rotor blades is not critical as it is balanced by the flow of cold gas from below.

Figure 12, an overall pressure distribution, shows only one notable feature, namely that the pressure at the first pressure boundary is nearly the same as that at the inlet.

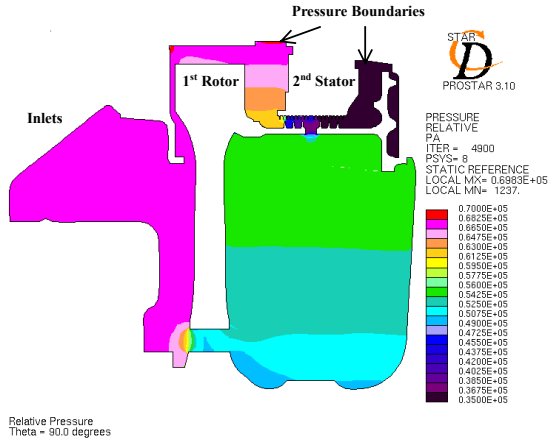

Figure 12: Fluid pressure

By not capturing the inter-disc drum conduction and conjugate heat transfer to the fluid, it is clear that the fluid temperature calculations are inaccurate in and around the labyrinth seal, as no thermal boundary layers exist there. This is, however, not necessarily the case for the discs themselves. Figure 13 shows the metal temperature of the first and second disc. At the contact points between the drum and the discs, the difference is as little as 50 K, therefore indicating some validity to the assumption that the effect of conduction through the drum is small and does not require modelling.

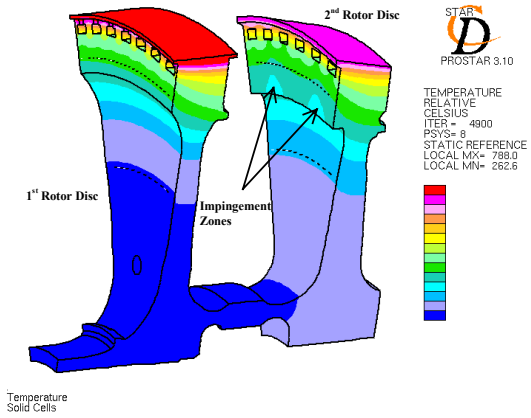

Figure 13: Metal temperature

Figure 13 reveals that there is a very strong temperature gradient at the top of the discs, and that the bulk of the disc material near the hub is maintained at relatively low temperatures. Cold spots on the upstream face of the second disc result from impingement through the holes in the inter-disc drum**.**

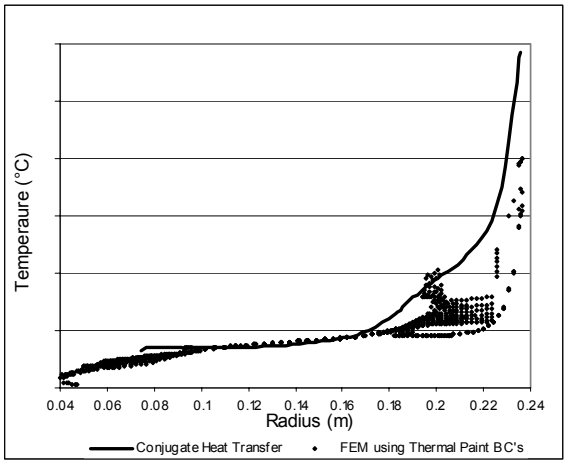

Figure 14: Comparison of conjugate and FEM/thermal paint results

Figure 14 compares results of surface temperature obtained from a Finite Element Analysis (FEA) using thermal paint results as boundary conditions and those from the conjugate heat transfer model under discussion. The results are encouraging, probably as conduction effects dominate the convection effects in the disc.

Disc Heat Transfer Coefficients

Figure 15 shows a plot of all the metal surfaces where heat transfer was calculated, with various detailed views. Y^+ values lie typically in the range 250 to 550 - much too high to expect accurate capturing of the boundary layer and subsequently heat transfer. However, the plot is at least qualitatively sound.

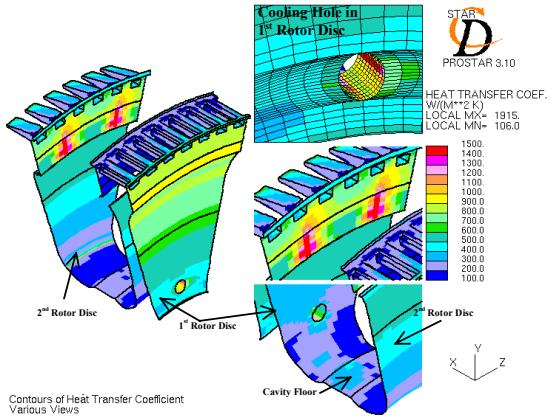

Figure 15: Heat transfer coefficients

Conclusions

The coolant flow through the turbine disc cavities of an engine geometry have been successfully modelled using the CFD package Star-CD. The solution includes simplified but accurate geometrical data, full conjugate heat transfer to the discs and accurate fluid properties thanks to the inclusion of various temperature based equations.

Despite reservations over mesh size, and in particular cell refinement near the wall leading to possible inaccuracies in the prediction of heat transfer, a realistic flow solution of a detailed disc cavity was obtained. At the same time heat transfer coefficients and temperature distributions were obtained and can be observed to be physical and in the correct order of magnitude, representing an advance on similar, earlier attempts of modelling disc cavity flows at Defencetek, while remaining a cost effective solution method for detailed disc cavity flows.

Acknowledgements

The author would like to thank Brian Cannoo for freely giving up his time and in-depth knowledge of Star-CD. He is responsible for the excellent quality of the post-processing.

Thomas Roos provided the boundary conditions and advised the author on what assumptions were valid. Philip Haupt provided the FEM data for results comparison.

References

CD Limited (1999) “User Guide Version 3.10”

NREC (1972), “Suite of design codes”

White F M (1991), “Viscous Fluid Flow,” Second Edition, McGraw Hill Inc.

Zucrow M J and Hoffman J D (1976), “Gas Dynamics,” Volume 1, John Wiley and Sons